Sleeper Contact Modelling in Asphalt Overlayment Trackbeds

Jørgensen, P.; Perslev, R.N.H.; Levenberg, E.

Published in:
Proceedings of 11th International Conference on the Bearing Capacity of Roads, Railways and Airfields

Link to article, DOI:
10.1201/9781003222910-22

Publication date:
2022

Document Version
Publisher's PDF, also known as Version of record

Eleventh International Conference on the Bearing Capacity of Roads, Railways and Airfields, Volume 3 – Hoff, Mork & Saba (eds)

Sleeper contact modelling in asphalt overlayment trackbeds

P. Jørgensen, R.N.H. Perslev & E. Levenberg*
Department of Civil Engineering, Section for Geotechnics and Geology, The Technical University of Denmark, Kongens Lyngby, Denmark

ABSTRACT: This study targeted the mechanics of asphalt overlayment trackbeds – a ballastless track type that mandates special wide-base sleepers equipped with a geotextile at the bottom. The objective was to develop an analytical model for quantifying how a geotextile and its compressibility properties influence the contact stress distribution at the sleeper-geotextile-asphalt interface. A nonlinear-hardening Winkler spring-bed was utilised to represent a geotextile, a rigid beam was utilised to represent a sleeper, and the pavement system was treated as an elastic half-space. Based on a parametric investigation of the new model it is concluded that the insertion of a geotextile at the sleeper-asphalt interface considerably affects the vertical stress distribution. The presence of a geotextile is shown to produce a more uniform stress distribution and eliminate excessively high contact stresses that would have developed near the sleeper perimeter. It is also shown that geotextile compression adds extra vertical flexibility to the track system with an order of magnitude similar to that of common rail pads. The developed model can handle realistic geotextile compressibility properties as well as any sleeper geometry; its analytical nature provides relative ease of replication for subsequent design and analysis.

Keywords: Ballastless asphalt tracks, Geotextile, Nonlinear Winkler spring-bed, Analytical modelling

1 INTRODUCTION

Conventional ballasted tracks are the most common trackbed type worldwide (Esveld, 2001). With the demand for faster, heavier, and more train passes, this standard track solution mandates increased frequency of repair activities, e.g., track realignment, ballast replacement, and sleeper replacement (Köllo, Puskás, & Köllo, 2015). The elevated maintenance effort led to the development of ballastless tracks based on Portland cement concrete – commonly known as slab track – offering improved track stability and reduced maintenance needs (Freudenstein, Geisler, Mölter, & Missler, 2018). Slab track is an established and accepted trackbed alternative in Germany, China, Japan, and South Korea, accommodating (especially) high-speed trains.

Another ballastless track alternative is asphalt overlayment. In this trackbed type, the sleepers with rails on top are supported over an asphalt pavement system, commonly composed of (top to bottom): several lifts of asphalt concrete, unbound aggregate base and subbase, and subgrade soil (or rock). In the absence of crib and shoulder ballast, and to safeguard track stability, asphalt overlayment involves special sleepers that are twice as wide and therefore twice as heavy compared to standard sleepers (Bose,

*Corresponding author
DOI: 10.1201/9781003222910-22

Levenberg, & Zania, 2018). Also, these special wide sleepers include a geotextile attached to their bottom; the geotextile is added to increase the contact area with the asphalt concrete surface, compensating for geometric unevenness at their interface. Potential advantages of this ballastless trackbed type include lower initial construction costs compared to a slab track solution, reduced noise and ground vibrations compared to both slab track and ballasted track, and reduced maintenance effort compared to a conventional track. Another advantage of using asphalt is environmental friendliness, given that the material is fully recyclable (NAPA, 2020).

Despite the above-mentioned merits, the asphalt overlayment idea is not widely accepted, with only a few full-scale applications – mostly inside tunnels within the German railway network (RailOne, 2011). Also, the mechanics of such a track solution is not deeply researched compared to ballasted tracks and slab tracks. Noteworthy studies in this context include the work of Lee et al. (2016) which experimentally evaluated an asphalt overlayment track with three different asphalt concrete thicknesses. The stated aim of the study was to identify an optimal structural cross-section; this was sought based on static loads applied to a full-scale mockup pavement, and subsequent observations of stress and strain responses within the structure. The study concluded that a 30 cm thick asphalt layer is optimal. Another relevant investigation was performed by Bose et al. (2018). The purpose of this work was to analyse track responses due to train braking. The analysis was purely analytic and focused on estimating the friction demand at a sleeper base that is required to resist longitudinal slippage during an emergency train braking event. For an asphalt overlayment solution, where the sliding resistance of the sleepers is solely supplied by a frictional mechanism at the base, it was shown that special heavy sleepers are needed to ensure lateral stability. In a recent investigation, Bose et al. (2018) experimentally analysed asphalt overlayment trackbeds based on full-scale instrumented sections loaded by a passing train. A numerical investigation accompanied the study focusing on horizontal strains and vertical stresses at the bottom of the asphalt concrete. However, the modelling did not consider a geotextile at the bottom of the sleepers. Lastly, Bose et al. (2021) reported on the development of a finite element model for asphalt overlayment tracks considering wide-base sleepers equipped with a geotextile at the bottom. The asphalt layer was modelled as linear viscoelastic, and the underlying unbound granular layer was treated as stress-dependent nonlinear-elastic; all other track layers and elements were treated as linear elastic. The model was calibrated and validated against measurements from a full-scale instrumented mockup excited by vertical loads: it was able to reproduce and predict a wide range of measured response traces due to different loading situations. Specifically, it was shown – both numerically and experimentally – that peak vertical deformations in the track structure were roughly composed of: 77% in the rail pad, 15% in the geotextile, and 6% in the unbound granular layer. The model of Bose et al. was elaborate and computationally heavy, requiring a large number of input parameters to execute.

The current study is motivated by the desire to further promote the asphalt overlayment solution; this is sought by contributing to an improved understanding of the system mechanics. Specifically, this paper aims to investigate the contact interaction between a single sleeper exposed to vertical loads (coming from the rails) and a supporting asphalt pavement system – when a geotextile is introduced at the interface. The objective is to develop a mechanistic model for quantifying how a geotextile and its compressibility properties influence the contact stress distribution at the sleeper-geotextile-asphalt interface. This development will be based on closed-form analytic formulations, and the paper aims to offer a step-by-step reproducible approach to all underlying equations. Unlike purely numerical methods, the reliance on analytical solutions is chosen to promote engineering utilisation and broaden the spectrum of applicability. Analytical solutions enable model parameters to accept a wide range of values without convergence concerns. The work also includes a narrow-scope parametric investigation, showcasing selected results and demonstrating some of the model capabilities.

2 CONTACT MODELLING

The problem considered hereafter deals with a single loaded sleeper, having a geotextile at the bottom, and resting on the surface of an asphalt pavement system. A plan view of this arrangement is shown in Figure 1a, and a cross-sectional view is shown in Figure 1b. As can be seen, the sleeper is a rectangular cuboid hosting a pair of rail pads. Train axle loads applied to the rails are transferred to the sleeper via these rail pads. The pavement system has three layers: asphalt concrete, aggregate base, and subgrade soil (or rock) extending to a large depth. The geotextile is a thin layer with an area that identically covers the sleeper's bottom.

The corresponding model is graphically presented in Figure 1c (plan view) and in Figure 1d (cross-sectional view). The sleeper is modelled as a weightless Euler-Bernoulli beam having infinite bending rigidity. Two identical point loads, each with intensity P, are applied at the position of the rail pads to represent the effects of a train axle. The pavement system is modelled as a half-space that is linear elastic, isotropic, homogeneous, and weightless. The geotextile is treated as a weightless nonlinear-hardening Winkler spring-bed residing in-between the beam and the half-space.

The aim of the modelling is to resolve the vertical stress distribution in the nonlinear Winkler spring-bed. This is sought through an iterative calculation-correction procedure wherein the stress distribution across the springs is first assumed uniform (iteration 0), and then applied to deform the half-space. This stress distribution is also, in a parallel calculation, applied to compress the springs from their initial length into a shorter (compressed) length. Next, the surface deflection of the half-space is added to the shortening of the springs, and the result of this addition is compared against a flat surface corresponding to the bottom of a rigid beam. Finally, the initial stress distribution assumption is refined such that the discrepancy with a perfectly flat surface is minimised. The refinement procedure is iterated until achieving satisfactory convergence.

To facilitate the calculations, the Winkler spring-bed, which covers the entire contact zone, is split into a large number of identical square areas numbered $n = 1 \ldots N$. The deflection (or vertical surface displacement) of the half-space during iteration i $(i = 0, 1, 2, \ldots)$ at the centre of any square area n is $\delta_n^{(i)}$; it is based on superposition:

$$\delta_n^{(i)} = \delta_{1,n}^{(i)} + \sum_{m=1}^{N} \delta_{2,m}^{(i)} \quad (m \neq n) \tag{1}$$

where $\delta_{1,n}^{(i)}$ and $\delta_{2,n}^{(i)}$ are based on Boussinesq's solution for a vertical force applied to the surface of a linear elastic half-space:

$$\delta_{1,n}^{(i)} = \frac{4 q_n^{(i)} a \left(1 - \nu^2\right) \ln\left(1 + \sqrt{2}\right)}{E \pi} \tag{2}$$

$$\delta_{2,n}^{(i)} = \frac{q_m^{(i)} a^2 \left(1 - \nu^2\right)}{E \pi r_{n,m}} \quad (m \neq n) \tag{3}$$

in which $\delta_{1,n}^{(i)}$ describes the half-space deflection at the centre of the n^{th} square (during iteration i) when it is loaded by a stress intensity $q_n^{(i)}$ while all other squares are not loaded, $\delta_{2,n}^{(i)}$ describes the half-space deflection (during iteration i) at the centre of the n^{th} square due to loading with stress intensity $q_m^{(i)}$ applied over the m^{th} square. Given the assumption of loading via a rigid beam, both $q_n^{(i)}$ and $\delta_n^{(i)}$ are always non-negative. The parameter $r_{n,m}$ denotes the distance between square n and square m whenever $m \neq n$. Both $q_n^{(i)}$ and $q_m^{(i)}$ differ from location to location depending on the stress distribution in the spring bed. The parameter a denotes the side-length of a square area, ν is Poisson's ratio of the half-space, and E is Young's modulus of the half-space. By repeating the above calculations for the entire contact area (i.e., for $n = 1 \ldots N$), the half-space deflection below the Winkler spring-bed is determined.

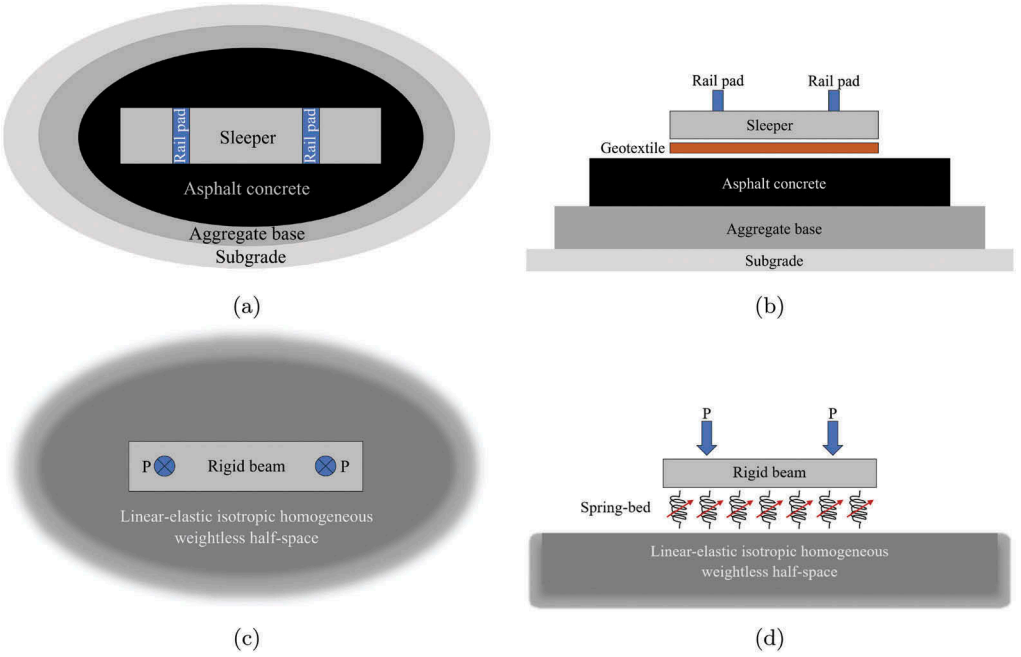

Figure 1. Sleeper-geotextile-pavement contact problem: (a) plan view of a sleeper resting on an asphalt pavement system, (b) cross-sectional view of a sleeper resting on an asphalt pavement system, (c) plan view of model, (d) cross-sectional view of model.

The next calculation step (during iteration i) targets the shortening of the spring-bed covering the n^{th} square. This shortening is also a non-negative entity; it is denoted by $\Delta_n^{(i)}$, and calculated based on Hooke's Law:

$$\Delta_n^{(i)} = \frac{q_n^{(i)}}{k_n^{(i)}} \tag{4}$$

wherein $k_n^{(i)}$ expresses the nonlinear stiffness of the Winkler spring-bed associated with the n^{th} square:

$$k_n^{(i)} = k_0 \left(1 + \frac{c\Delta_n^{(i)}}{t - \Delta_n^{(i)}} \right) \quad (t > \Delta_n^{(i)}) \tag{5}$$

where k_0 is the initial spring-bed stiffness (units of force per volume), t denotes the initial length of the spring-bed – analogous to the thickness of the geotextile when no train loads are applied to the rails, and c is a non-negative unitless parameter that governs the nonlinear-hardening behaviour of the spring-bed. As can be seen, if $c = 0$ then the spring-bed is linear, characterised by a constant stiffness k_0. For $c > 0$ this expression produces an ever increasing spring-bed stiffness as the shortening approaches the initial length t. In actuality, both the sleeper bottom and the asphalt surface are not perfectly flat. This means that the geotextile thickness (both initial and under train loading) will vary from location to location – bridging the irregularities in the contact area. Hence, all above-listed spring-bed properties represent average effective properties.

A graphical representation of Equation (5) is offered by Figure 2. The chart depicts the dependence of $k_n^{(i)}$ on the shorting $\Delta_n^{(i)}$ for four different values of k_0. As can be seen, for very

small shorting levels the spring-bed stiffness increases approximately linearly with respect to the shortening level. As the shortening gets closer to the initial length t, the spring-bed stiffness increases sharply and rapidly towards infinity. This model is deemed realistic, as it is practically impossible to compress a geotextile to zero thickness.

The iterative solution procedure of the contact problem advances with the aim of refining the stress intensity operating over each of the square areas, i.e., determining $q_n^{(i+1)}$. This is pursued by requiring that the upper-end of the Winkler spring-bed makes a perfectly flat surface – corresponding to the bottom of a rigid sleeper. In this context, the spring-bed upper-end surface elevation above the n^{th} square area is obtained by summing the half-space deflection $\delta_n^{(i)}$ with the spring-bed shortening $\Delta_n^{(i)}$. A perfectly flat upper surface means that all individual summations (i.e., for any n) yield the exact same result. In other words, that each individual summation is identical to the average over all summations. Based on this observation, it is possible to iteratively refine the stress intensity at the n^{th} square as follows:

$$q_n^{(i+1)} = q_n^{(i)} + \Delta q_n^{(i)} \tag{6}$$

where

$$\Delta q_n^{(i)} = \left(\underbrace{\left(\frac{1}{N} \sum_{n=1}^{N} \left(\Delta_n^{(i)} + \delta_n^{(i)} \right) \right)}_{A} - \underbrace{\beta \left(\Delta_n^{(i)} + \delta_n^{(i)} \right)}_{B} \right) k_n^{(i)} \tag{7}$$

in which the A term denotes the average over all summations, the B term is the individual summation, and their difference at the n^{th} square is multiplied by the spring-bed stiffness – corresponding to the n^{th} square – to provide the stress intensity refinement $\Delta q_n^{(i)}$. As all the springs approach a flat surface at the upper end, the difference between the A term and the B term decreases to zero. The outcome is that $\Delta q_n^{(i)}$ decreases to zero leading to $q_n^{(i)}$ approaching $q_n^{(i+1)}$. Iterations are stopped once convergence is attained, e.g., when $|\Delta q_n^{(i)}|$ is smaller than some predefined stress value (for all n's); another option is to stop the iterations when the absolute difference between the A and B terms is smaller than some predefined value (across all n's). The β parameter is a positive unitless multiplier introduced to facilitate the iteration procedure, either accelerate it ($\beta > 1$) or decelerate it ($\beta < 1$).

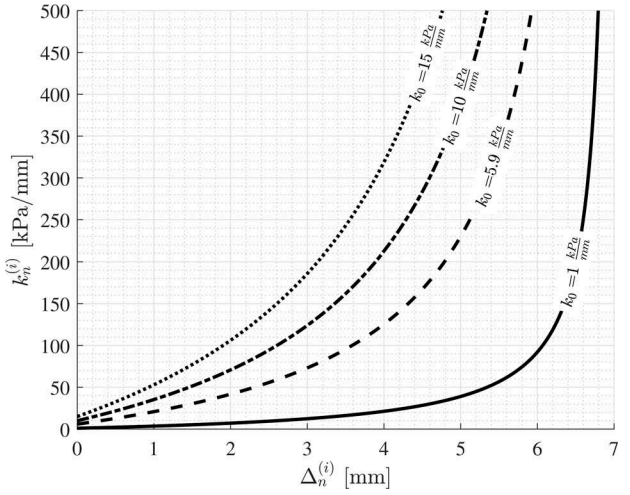

Figure 2. Graphical representation of the nonlinear-hardening Winkler spring-bed stiffness represented by Equation (5) with $t = 7$ mm and $c = 15$ for different k_0 values.

3 MODEL DEMONSTRATION

The aim here is to apply and demonstrate the proposed sleeper-geotextile-asphalt contact model. In this context, a narrow-scope parametric investigation is carried out involving a wide range of half-space moduli combined with a range of spring-bed properties covering several k_0 values with $c = 15$ and $t = 7$ mm. The later two parameters were chosen based on a laboratory characterisation of the geotextile currently utilised in the GETRAC A3 sleepers (RailOne, 2011).

The case considered hereafter deals with a wide sleeper that is 2.5 m long and 0.6 m wide; the overall loading intensity over this sleeper is 71 kN, i.e., P=35.5 kN (see Figure 1d). This intensity was chosen based on a separate analysis which included an infinitely long beam representing a UIC60 rail supported on a linear spring-bed or track modulus, and loaded by a point force of 100 kN representing one side of a single-axle carrying a total of 200 kN. With a track modulus of 50 MPa combined with a centre-to-centre sleeper spacing of 0.6 m (Bose & Levenberg, 2020), the maximal sleeper load is 35.5% of the axle load (hence 71 kN). Assumption of a track modulus, even though it considers a linear rail support, does not invalidate the analysis herein; it is merely a structured manner to arrive at a loading intensity applied to a single sleeper.

Figure 3 presents the contact conditions at the bottom of the sleeper for E=200 MPa and k_0=5.9 kPa/mm (and also $c = 15$ and $t = 7$ mm). The figure was prepared with a=10 mm (i.e., N=15000), $\beta = 0.5$, and 30 calculation iterations. The resulting maximal $|\Delta q_n^{(29)}|$ in Equation (6) was 0.3 kPa and the peak absolute difference between the A and B terms in Equation (7) was 9.7 microns. Shown in Figure 3a is a heat map of the stress distribution in the spring bed, i.e., $q_n^{(30)}$ in Equation (6). Contour lines of points experiencing identical stress level are included to facilitate the presentation. As can be seen, the overall distribution pattern is such that higher stresses concentrate around the sleeper edges. The contact stresses span a relatively narrow range, from 46 kPa to about 52 kPa with a mean stress value of 47.3 kPa and a standard deviation of 1.5 kPa. Shown in Figure 3b is a heat map of the spring-bed shortening (or geotextile compression), i.e., $\Delta_n^{(30)}$ in Equation (4). Contour lines are included – indicating points experiencing identical shortening. Overall, the shortening values span a relatively narrow range, from 1.50 mm to about 1.60 mm with a mean value of 1.55 mm and a standard deviation of 0.02 mm. As can be seen, the overall distribution pattern is such that slightly higher shortening concentrates near the sleeper edges.

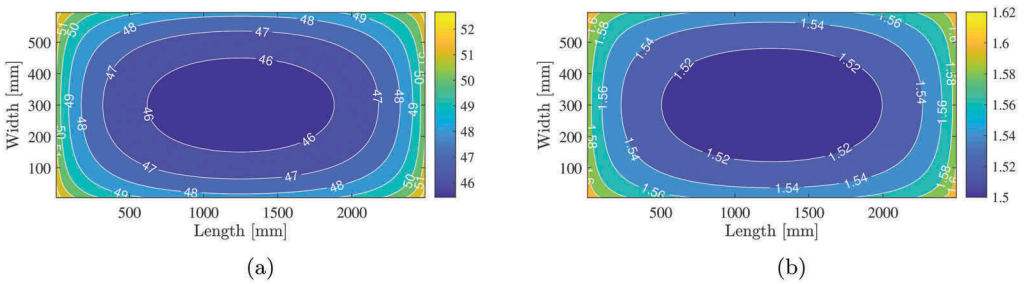

Figure 3. Contact conditions at the bottom of a wide sleeper with $E = 200$ MPa and k_0=5.9 kPa/mm: (a) vertical stress [kPa], and (b) geotextile compression [mm].

Investigated next is the standard deviation of the contact stress distribution, i.e., the standard deviation of $q_n^{(30)}$ for $n = 1 \ldots N$. This entity is hereafter denoted by σ; it encapsulates in a single parameter the influence of the geotextile on the prevailing contact conditions. Without introducing a geotextile at the sleeper-pavement interface, the vertical stress distribution is expected to be highly non-uniform – as model stresses would tend to infinity at the sleeper edges. On the other hand, insertion of a geotextile at the sleeper-pavement interface eliminates

the infinite stresses at the edges and produces a more even stress distribution – associated with a smaller σ.

Figure 4a offers a semi-log plot of σ against E for three levels of the initial spring-bed stiffness k_0. The half-space modulus (depicted on the abscissa) spans the range 100 MPa to 40000 MPa. This range was chosen to encapsulate the two extreme moduli values that asphalt concrete may experience. The low-end is associated with the material's equilibrium modulus approached at very high temperatures while the high-end value is associated with the material's instantaneous modulus approached at very low temperatures Levenberg, 2020). As can be seen in the chart, there is a monotonous decrease in σ as the half-space modulus increases, indicating an improvement in contact stress uniformity and therefore an increase in the geotextile's effectiveness. The chart also shows that for a given half-space modulus, smaller k_0 values improve the contact stress uniformity.

Figure 4b offers a semi-log plot of σ against k_0 for three levels of the half-space modulus: 200 MPa, 2000 MPa, and 20000 MPa. The initial spring-bed coefficient (depicted on the abscissa) spans the range 0.01 kPa/mm to 20 kPa/mm. As can be seen in the chart, as k_0 increases in value for a given E, σ first decreases slightly, and then increases monotonically towards some horizontal asymptote. The chart also shows that for a given k_0 value, a larger half-space modulus improves the contact stress uniformity (drop in σ); this effect is very pronounced, exhibiting high dependence upon the modulus level.

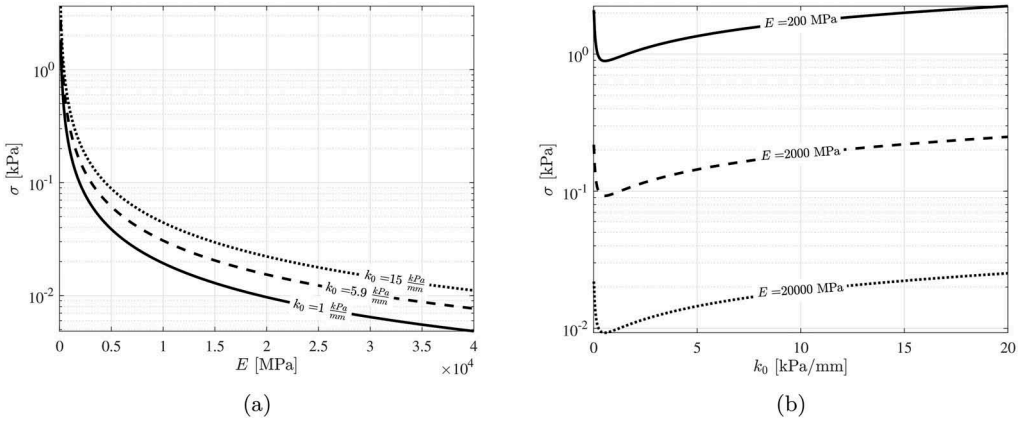

Figure 4. Dependence of σ, the standard deviation of the contact stress distribution, upon: (a) the half-space modulus for different k_0 values, and (b) the initial spring-bed stiffness for different E values.

4 CONCLUSION

This study targeted the mechanics of asphalt overlayment trackbeds, focusing on the sleeper-geotextile-asphalt contact interaction under quasi-static train loading conditions. An iterative analytical model was proposed (see Section 2) to estimate the geotextile compression (see Equation (4)) and the associated vertical stress distribution (see Equation (6)). The work also included a narrow-scope parametric investigation in which the model was applied to generate some results with realistic input parameters (see Section 3). A nonlinear-hardening Winkler spring-bed was utilised to represent the geotextile (see Equation (5)); treatment of the sleeper and pavement system involved more radical modelling simplifications: sleeper as a rigid beam and pavement system as an elastic half-space (see Figure 1).

It is concluded that the insertion of a geotextile at the sleeper-asphalt interface considerably affects the vertical stress distribution. The presence of a geotextile produces a more uniform stress distribution, and eliminates excessively high contact stresses that would have developed

near the sleeper perimeter. The significance of this is that the presence of a geotextile limits sleeper spalling damage along the edges, and also limits mechanical indentation of the asphalt surface.

Given that the geotextile is compressed (i.e., thickness is shortened) under train loadings, extra vertical flexibility of the rail support is introduced into the track system. The shortening is expected to be of the same order of magnitude as the compression of common rail pads. This result coincides with the behaviour exhibited in full-scale tests, as reported by Bose et al. (2021). Nonetheless, the proposed model mandates a more direct and targeted experimental validation. One approach to achieve this is measuring the geotextile compression at the sleeper perimeter – as was done Bose et al. (2020). Another model validation approach is placing a pressure sensitive film (Liggins et al. (1995)) in contact with the geotextile.

Ultimately, the model proposed herein can accept and handle realistic geotextile compressibility properties; as such, it can support the choice of geotextile properties in a given situation. In effect, the model is material agnostic, which means that it can potentially apply to under sleeper pads (which are becoming common in ballasted tracks). Also, the model can accept and handle any sleeper geometry, i.e., the formulation is not restricted to a rectangular contact area. Lastly, the utilisation of closed-form analytic solutions ensures superior numerical stability and ease of replication for subsequent engineering application.

REFERENCES

Bose, T., & Levenberg, E. (2020). A priori determination of track modulus based on elastic solutions. *KSCE Journal of Civil Engineering*, *24*(10), 2939–2948.

Bose, T., Levenberg, E., & Zania, V. (2018). Analyzing track responses to train braking. *Proceedings of the Institution of Mechanical Engineers, Part F: Journal of Rail and Rapid Transit*, *232* (7), 1984–1993.

Bose, T., Levenberg, E., & Zania, V. (2021). Numerical modeling of a ballastless track mockup based on asphalt. *Construction and Building Materials*, *274*(121852), 1–18.

Bose, T., Zania, V., & Levenberg, E. (2020). Experimental investigation of a ballastless asphalt track mockup under vertical loads. *Construction and Building Materials*, *261*, 119711.

Esveld, C. (2001). *Modern railway track*. MRT–Productions.

Freudenstein, S., Geisler, K., Mölter, T., & Missler, M. (2018). *Ballastless tracks*. John Wiley & Sons.

Köllo, S. A., Puskás, A., & Köllo, G. (2015). Ballasted track versus ballastless track. In *Key engineering materials* (Vol. 660, pp. 219–224).

Lee, S.-H., Choi, Y.-T., Lee, H.-M., & Park, D.-W. (2016). Performance evaluation of directly fastened asphalt track using a full-scale test. *Construction and Building Materials*, *113*, 404–414

Lee, S.-H., Park, D.-W., Vo, H. V., & Fang, M. (2019). Analysis of asphalt concrete track based on service line test results. *Construction and Building Materials*, *203*, 558–566.

Levenberg, E. (2020). *Pavement mechanics – lecture notes*. Eyal Levenberg - Danish Publisher 972317. doi: 10.11581/dtu:00000088

Liggins, A., Hardie, W., & Finlay, J. (1995). The spatial and pressure resolution of fuji pressuresensitive film. *Experimental Mechanics*, *35*(2), 166–173.

NAPA. (2020). *Asphalt for recycling and energy reduction*. Retrieved 3-15-2020, from https://www.asphaltpavement.org/index.php?option=com_content&view=article&id=201&Itemid=774

RailOne. (2011). *Getrac, the ballastless track system on asphalt*. Rail.One. Retrieved from https://www.railone.com/fileadmin/daten/05-presse-medien/downloads/broschueren/en/Getrac_EN2012_ebook.pdf